Comparative ^{18}F-FDG PET of Experimental *Staphylococcus aureus* Osteomyelitis and Normal Bone Healing

Jyri K. Koort, MD[1]; Tatu J. Mäkinen, MD[1]; Juhani Knuuti, MD, PhD[2]; Jari Jalava, PhD[3]; and Hannu T. Aro, MD, PhD[1]

[1]Orthopaedic Research Unit, Department of Surgery, University of Turku, Turku, Finland; [2]Turku PET Centre, University of Turku, Turku, Finland; and [3]Department of Human Microbial Ecology and Inflammation, National Public Health Institute, Turku, Finland

PET using ^{18}F-FDG is a promising imaging modality for bone infections, based on intensive consumption of glucose by mononuclear cells and granulocytes. The method may have limitations in distinguishing uncomplicated bone healing from osteomyelitis. Bone healing involves an inflammatory phase that represents a highly activated state of cell metabolism and glucose consumption, mimicking infection on PET images. This laboratory study of a standardized model was designed to compare the ^{18}F-FDG PET characteristics of normal bone healing with those of local osteomyelitis. **Methods:** A localized osteomyelitis model of the rabbit tibia was created by modifying a previously reported canine model. In the osteomyelitic group ($n = 8$), a standardized metaphyseal defect of the proximal right tibia was surgically created and filled with a block of orthopedic bone cement, followed by injection of a predetermined amount (0.1 mL) of *Staphylococcus aureus* (strain 52/52A/80, 1×10^5/mL) into the space around the cement. The control group of animals with normal bone healing ($n = 8$) underwent the same procedure, but the bacterial injection was replaced by a sterile saline injection. The bone cement was surgically removed during debridement at 2 wk. Osteomyelitis was confirmed with positive bacterial cultures during the debridement and 6 wk later at the time of sacrifice. ^{18}F-FDG PET and peripheral quantitative CT were performed 3 and 6 wk after the debridement. The presence of osteomyelitic bone changes on plain radiographs was classified according to a previously published system. **Results:** Before surgery, the standardized uptake values of ^{18}F-FDG did not differ markedly between the right and left tibias. In the control animals, uncomplicated bone healing was associated with a temporary increase in ^{18}F-FDG uptake at 3 wk ($P = 0.007$), but it returned almost to normal by 6 wk. In the experimental animals, localized osteomyelitis resulted in an intense continuous uptake of ^{18}F-FDG, which was higher than that of healing and intact bones at 3 wk ($P = 0.014$ and $P < 0.001$, respectively) and at 6 wk ($P < 0.001$). **Conclusion:** ^{18}F-FDG PET seems to be an efficient tool in the differentiation of uneventful bone healing from bone healing complicated by localized osteomyelitis.

Received Dec. 22, 2003; revision accepted Feb. 12, 2004.

For correspondence or reprints contact: Hannu T. Aro, MD, PhD, Department of Surgery, University of Turku, FIN-20520 Turku, Finland.

E-mail: hannu.aro@utu.fi

Key Words: infectious disease; PET; osteomyelitis; bone healing; rabbit

J Nucl Med 2004; 45:1406–1411

Imaging of deep bone infections remains challenging for 2 reasons. First, MRI has not proved to be as superior as initially believed. MRI provides excellent anatomic detail but is of limited value in the presence of metallic implants and in discriminating between edema and active infection after surgery (*1*). Second, we still lack adequate imaging modalities to follow the response of infected bones to antibacterial treatment.

Early clinical experience suggests that PET using ^{18}F-FDG may be promising for imaging bone infections (*2*,*3*). PET offers more accurate information for diagnosing infection than do conventional nuclear medicine procedures (*4*).

^{18}F-FDG PET has certain potential limitations as a tool for diagnosing bone infection. The method is based on intensive use of glucose by mononuclear cells and granulocytes. Previous animal studies have shown that ^{18}F-FDG uptake increases both in bacterial infections (*5*) and in aseptic inflammatory processes (*6*). The problem is that early bone healing involves an inflammatory phase that represents a highly activated state of cell metabolism and glucose consumption (*7*), mimicking infection on PET images. It has been proposed that an interval of 3–6 mo should be allowed before PET to minimize the risk of false-positive findings during initial stages of postsurgical and traumatic bone healing (*2*).

This study was designed to compare the ^{18}F-FDG PET characteristics of normal bone healing with those of bone infection under standardized laboratory conditions. Specifically, we addressed the following questions: How quickly does ^{18}F-FDG activity return to the baseline level during normal bone healing, and does ^{18}F-FDG PET allow discrimination of bone infection from early bone healing?

MATERIALS AND METHODS

Animals

Sixteen adult male New Zealand White rabbits (Harlan) weighing 2.5–3.5 kg were used. Before surgery, the rabbits were acclimated to their new environment and fed a standard laboratory diet. They were caged individually at a constant ambient temperature. The Ethical Committee of the University of Turku and the Provincial State Office of Western Finland approved the study protocol. All experiments were carried out in accordance with the guidelines of the local Animal Welfare Committee.

Study Protocol

For baseline values, ^{18}F-FDG PET was performed on 4 animals before surgery to confirm that tracer uptake was equal in the right and left tibias. For the comparative study, the animals were divided into 2 groups: the osteomyelitic group ($n = 8$) and the healing-bone group ($n = 8$). In both groups, each animal underwent a 2-stage surgery involving the application of a small block of preshaped bone cement in a standardized defect of the right proximal tibia followed by debridement surgery 2 wk later. In the osteomyelitic group, application of the bone cement was associated with injection of a predetermined dose of *Staphylococcus aureus* suspension, inducing constant localized osteomyelitis. In the healing-bone group, the defect was allowed to heal uneventfully after removal of the bone cement. Comparative quantitative ^{18}F-FDG PET and peripheral quantitative CT (pQCT) were performed 3 and 6 wk after the debridement surgery. Osteomyelitis was confirmed by cultures positive for bacteria during the debridement and at the time of sacrifice. The process of osteomyelitis and the process of uncomplicated bone healing were also compared using radiography and hard-tissue histology.

Induction of Infection (First Stage of Surgery)

The localized osteomyelitis model (stage IIIA in the classification of Cierny et al. (*8*)) was modified from the canine model of Fitzgerald (*9*). The animals were premedicated with a subcutaneous injection of 1 mg of atropine (Atropin; Leiras Oy) per kilogram of body weight. Anesthesia was induced using a subcutaneous injection of 0.3 mL of fentanyl citrate (0.315 mg/mL) and fluanisone (10 mg/mL) (Hypnorm; Janssen Pharmaceutica) per kilogram of body weight. Before surgery, another injection of 0.2–0.4 mL of fentanyl citrate-fluanisone per kilogram was given. Using sterile surgical conditions, a cortical bone window of 6 × 2.7 mm was drilled under saline cooling into the proximal medial metaphysis of the right tibia. Bone marrow was removed with saline lavage, and the defect was filled with a small block of polymerized bone cement (Palacos R-40; Schering-Plough). The bone cement acted as a foreign body for infection. The periosteal and fascial layers were closed over the cortical defect. Subsequently, 0.1 mL of 1×10^5 colony-forming units of *Staphylococcus aureus* (strain 52/52A/80, kindly provided by Dr. Jon T. Mader) was injected into the space surrounding the bone cement. In control animals (healing-bone group), 0.1 mL of sterile saline was injected into the corresponding space. Finally, the skin wound was closed in layers, and an intramuscular injection of 0.1 mg of naloxone (Narcanti; Du Pont Pharmaceuticals Ltd.) per kilogram of body weight was given. Preoperatively, a single prophylactic dose of 500,000 IU of benzylpenicillin (GeePen; Orion Pharmaceuticals) was given intramuscularly to the control animals. After surgery, the animals were closely monitored. Functional activity was not limited. The animals received standard postoperative pain medication (4 mg of carprofen [Rimadyl Vet; Pfizer, Vericore Ltd.] per kilogram of body weight) for 3 d.

Debridement (Second Stage of Surgery)

Two weeks after the initial surgery, all animals underwent the second stage of surgery. Using the previous surgical approach, the defect area was exposed and swab cultures were taken to confirm that the clinical induction of staphylococcal bone infection had been successful. The swab specimens were cultured for 20 h at 35°C in blood agar plates. The bone cement was removed and separately cultured for 4 d at 35°C on brain heart infusion solution (BBL; Becton Dickinson Microbiology Systems). The defect space was lavaged with saline. Any necrosis of soft tissues was surgically excised. After debridement, the wound was closed in layers. Postsurgical care and mobilization were the same as for the initial procedure.

PET

^{18}F-FDG PET of each animal was performed 3 and 6 wk after the second stage of surgery (Fig. 1).

^{18}F-FDG was synthesized with an automatic apparatus by a modification of the method of Hamacher et al. (*10*), leading to a specific activity > 75 GBq·μmol^{-1} and a radiochemical purity $> 99\%$.

PET was performed using an Advance whole-body scanner (General Electric Medical Systems), which acquires 35 contiguous slices with an axial field of view of 15.2 cm (*11*). The slice thickness of the scanner was 4.25 mm, and the spatial resolution was 5 mm in full width at half maximum in the center of the field of view.

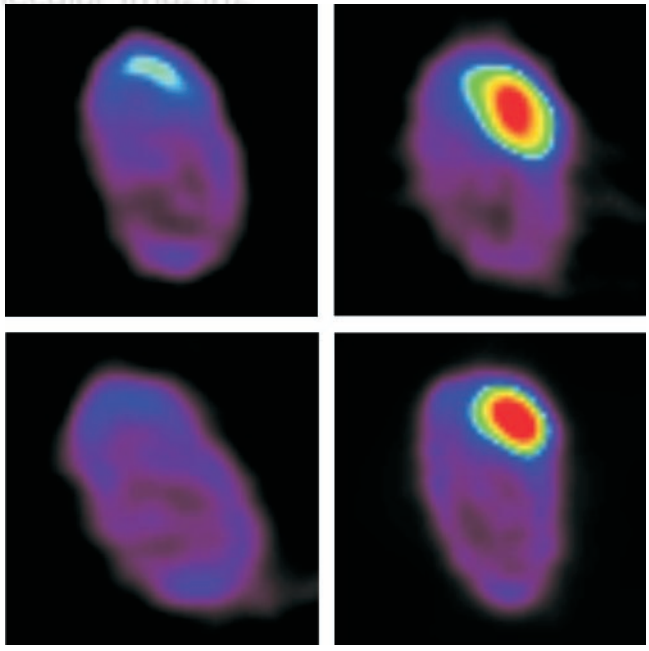

FIGURE 1. Sequential ^{18}F-FDG PET images of rabbit tibias at 3 and 6 wk (top and bottom, respectively). In the control animal (left), the healing-bone region shows a marked decrease in ^{18}F-FDG activity by 6 wk (SUV ratios, 1.9 and 1.2 at 3 and 6 wk, respectively). In the experimental animal (right), the corresponding bone region with osteomyelitis shows continuous ^{18}F-FDG uptake (SUV ratios, 3.1 and 5.5 at 3 and 6 wk, respectively).

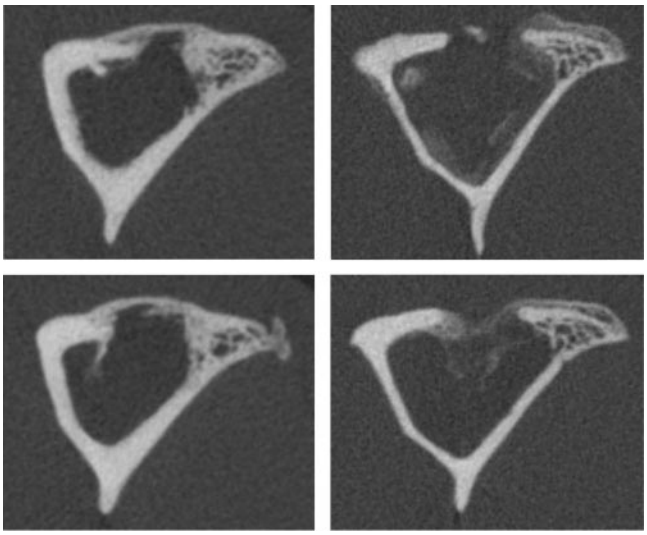

FIGURE 2. Sequential pQCT images of rabbit tibias at 3 and 6 wk (top and bottom, respectively). In the control animal (left), closure of the cortical window is already seen at 3 wk. In the experimental animal, with an osteomyelitic bone (right), no apparent closure of the cortical window is seen at 3 wk and the cortical window is still open at 6 wk.

For PET, the animals were sedated using the same method as was used for anesthesia during the first stage of surgery. A mean of 93 MBq of ^{18}F-FDG (range, 85–105 MBq) was injected into the ear artery. The animals were not kept fasting before ^{18}F-FDG administration. Hyperglycemia is known to reduce ^{18}F-FDG uptake by tumor cells, but it may not have a negative effect on ^{18}F-FDG uptake in inflammatory cells (*12*). A dynamic acquisition consisting of four 5-min frames and lasting 20 min was started 40 min after the ^{18}F-FDG injection. A 5-min transmission scan for attenuation correction was obtained after the emission imaging, using 2 rod sources containing ^{68}Ge.

PET Data Analysis

Data were corrected for dead time, decay, and photon attenuation, and the images were reconstructed in a 128 × 128 matrix using a Hanning filter with a cutoff frequency of 4.6 mm. Quantitative analysis was performed on standardized circular regions of interest (ROIs) (r = 3.8 mm) over the defect area of the right tibia and the corresponding region of the contralateral intact left tibia. The average radioactivity concentration in an ROI was used for comparative analysis of the 2 sides. ^{18}F-FDG accumulation was reported as the standardized uptake value (SUV), which was calculated as the radioactivity of the ROI divided by the relative injected dose, expressed per kilogram of body weight. In addition, the activity ratios between the operated and nonoperated sides were calculated (*13*). During PET image analysis, the pQCT image of each bone was used as a reference for the constant anatomic positioning of the ROIs.

pQCT

Aside from undergoing PET, each animal underwent pQCT 3 and 6 wk after the second stage of surgery (Fig. 2).

With the animal under sedation, the right hind limb was placed in a holder and imaged with a Stratec XCT Research M pQCT device (Norland Stratec Medizintechnik GmbH). After an initial scout view had been obtained, 6 consecutive cross-sectional images with a slice distance of 0.75 mm and a voxel size of 0.092 × 0.092 × 1.25 mm were obtained in the horizontal plane at the bone defect.

Radiography and Histology

The animals were sacrificed by intravenous administration of sodium pentobarbital (Mebunat; Orion) 6 wk after the debridement. Using sterile technique, the area of the bone defect was exposed and swab cultures were taken both from the bone defect itself and from the surrounding soft tissues to confirm the presence of persistent staphylococcal bone infection.

After the cultures had been obtained, the specimens were subjected to radiography using an Alpha RT mammography device (Instrumentarium Corp.) (Fig. 3). The radiographic presence of osteomyelitic bone changes was classified according to the osteomyelitis system of Mader and Wilson (grades 0–4) (*14*).

For the histologic analysis, separate specimens were prepared from the bone segment and surrounding soft tissues. The bone specimens were fixed in 70% ethanol, dehydrated in a graded series of ethanol, cleared in xylene, and embedded in isobornyl methacrylate (Technovit 1200 VLC; Kulzer). With the use of a water-cooled, high-speed, low-feed saw equipped with a diamond-impregnated blade, specimens were cut in the cross-sectional plane at the center of the cortical window.

Statistical Analysis

The significance of differences in SUVs between osteomyelitic bones, healing bones, and intact bones was calculated using 1-way ANOVA with a post hoc Tukey test. Within each group, ^{18}F-FDG activity at 3 wk was compared with that at 6 wk using the Student paired t test. The results of the radiographic scorings and pQCT

FIGURE 3. Plain radiographs demonstrating a healing defect (arrow) of the proximal tibia in a control animal (left) and a localized osteomyelitic defect (arrows) in an experimental animal (right).

measurements were analyzed by a nonparametric test and by 1-way ANOVA with a post hoc Tukey test, respectively. A *P* value of 0.05 was considered significant. All statistical analyses were conducted using SPSS statistical software (version 11.5; SPSS Inc.).

RESULTS

Confirmation of Staphylococcal Infection

In the osteomyelitic group, all bacterial cultures taken from the bone and foreign body (bone cement) during debridement surgery were positive for inoculated *Staphylococcus aureus* (strain 52/52A/80). In the healing-bone group, none of the corresponding cultures were positive.

At the time of sacrifice, bacterial cultures of the osteomyelitic group remained positive for the same strain of *Staphylococcus aureus*. In 3 animals, cultures of the surrounding soft tissues were also positive for the same pathogen. In the healing-bone group, cultures of the bone and the soft tissues remained negative for bacteria.

PET of Osteomyelitic and Healing Bone

Preoperative ^{18}F-FDG PET findings did not significantly differ between the 2 sides (ROIs in the right and left tibias). The SUV of intact bone was 0.35 (SD, 0.06), and the SUV ratio of the 2 sides was 1.02 (SD, 0.04).

Uptake of ^{18}F-FDG by healing bone had increased significantly ($P = 0.007$) by 3 wk (Fig. 4) but returned almost to normal by 6 wk; at that time, uptake by healing bone did not differ significantly ($P = 0.865$ for SUV ratio) from uptake by intact bone. The SUVs of the healing bones varied from 0.51 to 1.21 (mean, 0.74; SD, 0.20) at 3 wk and from 0.30 to 0.96 (mean, 0.51; SD, 0.13) at 6 wk. The SUV ratio was 2.35 (SD, 0.26) at 3 wk and 1.32 (SD, 0.54) at 6 wk.

In the osteomyelitic group, ^{18}F-FDG activity was significantly higher ($P < 0.001$) in the infected region than in intact bone at both 3 and 6 wk. Uptake was also significantly higher in the osteomyelitic region than in healing bone at both 3 wk ($P = 0.014$) and 6 wk ($P < 0.001$). Unlike healing bones, osteomyelitic bone regions did not show a marked decrease in ^{18}F-FDG activity over time. The SUVs of the osteomyelitic regions varied from 0.84 to 2.79 (mean, 1.95; SD, 0.71) at 3 wk and from 0.76 to 2.89 (mean, 1.69; SD, 0.85) at 6 wk. The SUV ratios varied from 2.2 to 7.6 (mean, 3.90; SD, 1.74) at 3 wk and from 2.8 to 5.5 (mean, 4.19; SD, 0.99) at 6 wk. The 3 animals with extension of bone infection into soft tissues, confirmed by positive bacterial cultures, showed local spread of ^{18}F-FDG activity outside the bone. However, these animals did not show higher bone ^{18}F-FDG activity than did those with infection limited to the medullary cavity.

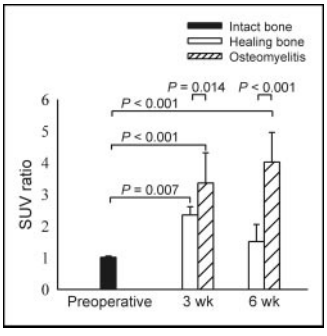

FIGURE 4. ^{18}F-FDG activity in intact bones, healing bone defects, and osteomyelitic regions. SUV ratios were calculated between operated and nonoperated sides.

Radiography, pQCT, and Histology

In the osteomyelitic group, plain radiographs at 6 wk showed localized osteomyelitis with moderate bone destruction. According to the osteomyelitis scoring system of Mader and Wilson (grades 0–4) (*14*), the mean score was 3.43 (SD, 0.54) in the osteomyelitic group and 0.25 (SD, 0.46) in the healing-bone group ($P < 0.01$).

In addition to the hard-tissue histologic sections, pQCT imaging allowed cortical window closure to be measured as a function of the healing time. In the healing-bone group, the cortical window had closed, on average, to 58% (SD, 23%) of its original length by 3 wk and to 77% (SD, 26%) by 6 wk. In the osteomyelitic group, no apparent closure of the cortical window had occurred by 3 wk. At 6 wk, the cortical window had closed, on average, to 33% (SD, 34%) of its original length. Differences between the groups were not statistically significant.

DISCUSSION

^{18}F-FDG, the most commonly used PET tracer for diagnosis of infection (*2*), has been shown to localize autoradiographically in the regions with the highest numbers of macrophages and polymorphonuclear leukocytes (*5*). This study evaluated the ^{18}F-FDG PET characteristics of bone healing and infection in a standardized infection model. Of particular interest for clinical work was the exploration of whether bone infection could be distinguished from normal bone healing. The results showed that intact bones have low ^{18}F-FDG uptake, whereas early stages of normal bone healing (without infection) were associated with transiently increased uptake, which tended to normalize within 6 wk. Bone infection was associated with an intense, continuous ^{18}F-FDG uptake. On the basis of these findings, the process of bone healing could be distinguished from bone infection using ^{18}F-FDG PET.

The early stages of bone healing, involving an inflammatory phase with a highly activated state of cell metabolism and glucose consumption, may mimic infection on PET images (*15*). Fresh fractures are known to have high ^{18}F-FDG uptake (*16*). In 2 ^{18}F-FDG PET studies of suspected osteomyelitis, uptake related to postsurgical bone healing produced false-positive results (*13*,*17*). In a study of 22 patients, ^{18}F-FDG PET allowed a correct diagnosis of osteomyelitis in 6 patients, whereas 2 patients with recent osteotomy showed false-positive uptake (*17*). In another study—of 60 patients with suspected osteomyelitis—^{18}F-

FDG PET allowed correct identification of osteomyelitis in 25 patients, but 2 patients of 4 with false-positive findings had undergone bone surgery less than 6 mo before being imaged with PET (*13*). These clinical observations suggest that an interval of 3–6 mo between surgery and PET should be allowed to minimize the risk of false-positive findings during early stages of postsurgical and traumatic bone healing (*2*). A recent retrospective analysis of 37 patients also suggested that an abnormal accumulation of ^{18}F-FDG at a fracture site for longer than 3 mo is likely due to either osteomyelitis or other pathologic processes, such as malignancy (*18*).

The localized osteomyelitis model (stage IIIA according to the classification of Cierny et al. (*8*)) adopted in the current experiment was modified from a canine model described by Fitzgerald (*9*) and by Calhoun and Mader (*19*). There are well-known difficulties in the induction of bone infection in rabbits (*20*). A high inoculum of bacterial organisms is required to produce osteomyelitis in rabbits, increasing animal mortality. In most osteomyelitis rabbit models, sodium morrhuate, a mild sclerosing agent causing aseptic bone necrosis, has been used to promote progressive osteomyelitis and to decrease the necessary inoculum of bacteria for infection. However, the use of sodium morrhuate in the induction of bone infection has certain disadvantages (*20*). Sodium morrhuate may result in diffuse osteomyelitis (stage IVA according to the classification of Cierny et al.) of the rabbit tibia. In the model of Fitzgerald, originally developed for the canine tibia, a block of bone cement is inserted into the intramedullary canal to produce a biomaterial-related infection. This approach allows lowering of the inoculum of bacteria required for osteomyelitis, decreasing mortality. The model, applicable also in the rabbit tibia as shown in this experiment, has several advantages. The osteomyelitis is relatively easy to produce and is localized.

The current model was based on the use of *Staphylococcus aureus* as the bone pathogen. *Staphylococcus aureus* is the most frequently encountered microorganism in any type of clinical osteomyelitis (*21*). There are also other clinically important and increasingly isolated bone pathogens that may produce less severe infection than *Staphylococcus aureus*. The indolent clinical picture of bone infections caused by *Staphylococcus epidermidis* is well known. Under experimental conditions, osteomyelitis caused by *Pseudomonas aeruginosa* also produced less destructive infection than did *Staphylococcus aureus* osteomyelitis (*22*). It is well anticipated that in these low-grade bone infections, ^{18}F-FDG uptake may be different from that caused by *Staphylococcus aureus*. Therefore, further studies of different bacteria are advocated.

Our study also had other limitations. The results were applicable only to the experimental model studied. The time required for increased ^{18}F-FDG activity to appear at the site of a healing bone might depend on the location and type of skeletal injury. For example, spontaneous osteoporotic compression fractures of the spine tend to have normal ^{18}F-FDG uptake, whereas pathologic vertebral fractures are highly positive for uptake on PET scans (*23*). The applied experimental model represents chronic bone infection. Although distinction between acute and chronic processes has not been necessary in clinical staging of adult deep bone infections (*8*), our results may not be applicable to acute bone infections in the absence of underlying bone disease.

The animal model that we used is amenable to local antibiotic therapy and various surgical treatments. Most important, our findings suggest the feasibility of using ^{18}F-FDG PET for following up the progress of osteomyelitis. The same technique might prove to be invaluable for noninvasive evaluation of the response of osteomyelitis to treatment, not only under experimental conditions but also in clinical patients.

CONCLUSION

^{18}F-FDG PET is one of the most promising imaging modalities for diagnosis of deep bone infections, but clinical experience suggests that recent bone surgery or a fresh bone fracture may cause false-positive findings. In this study of a standardized rabbit osteomyelitis model, we showed that bone infection could be distinguished from bone healing.

ACKNOWLEDGMENTS

This work was funded by grants from the National Technology Agency, Finland (TEKES). Two of the authors are supported PhD students of the Finnish Graduate School for Musculoskeletal Diseases. The authors acknowledge Tero Vahlberg for statistical consultation.

REFERENCES

1. Ledermann HP, Kaim A, Bongartz G, Steinbrich W. Pitfalls and limitations of magnetic resonance imaging in chronic posttraumatic osteomyelitis. *Eur Radiol.* 2000;10:1815–1823.
2. De Winter F, Vogelaers D, Gemmel F, Dierckx RA. Promising role of 18-F-fluoro-D-deoxyglucose positron emission tomography in clinical infectious diseases. *Eur J Clin Microbiol Infect Dis.* 2002;21:247–257.
3. Kälicke T, Schmitz A, Risse JH, et al. Fluorine-18 fluorodeoxyglucose PET in infectious bone diseases: results of histologically confirmed cases. *Eur J Nucl Med.* 2000;27:524–528.
4. Guhlmann A, Brecht-Krauss D, Suger G, et al. Fluorine-18-FDG PET and technetium-99m antigranulocyte antibody scintigraphy in chronic osteomyelitis. *J Nucl Med.* 1998;39:2145–2152.
5. Sugawara Y, Gutowski TD, Fisher SJ, Brown RS, Wahl RL. Uptake of positron emission tomography tracers in experimental bacterial infections: a comparative biodistribution study of radiolabeled FDG, thymidine, L-methionine, ^{67}Ga-citrate, and ^{125}I-HSA. *Eur J Nucl Med.* 1999;26:333–341.
6. Yamada S, Kubota K, Kubota R, Ido T, Tamahashi N. High accumulation of fluorine-18-fluorodeoxyglucose in turpentine-induced inflammatory tissue. *J Nucl Med.* 1995;7:1301–1306.
7. Einhorn TA. The cell and molecular biology of fracture healing. *Clin Orthop.* 1998;355(suppl):S7–S21.
8. Cierny G III, Mader JT, Penninck JJ. A clinical staging system for adult osteomyelitis. *Contemp Orthop.* 1985;10:17–37.
9. Fitzgerald RH Jr. Experimental osteomyelitis: description of a canine model and the role of depot administration of antibiotics in the prevention and treatment of sepsis. *J Bone Joint Surg Am.* 1983;65:371–380.

10. Hamacher K, Coenen HH, Stocklin G. Efficient stereospecific synthesis of no-carrier-added 2-[^{18}F]-fluoro-2-deoxy-D-glucose using aminopolyether supported nucleophilic substitution. *J Nucl Med.* 1986;27:235–238.
11. DeGrado TR, Turkington TG, Williams JJ, Stearns CW, Hoffman JM, Coleman RE. Performance characteristics of a whole-body PET scanner. *J Nucl Med.* 1994;35:1398–1406.
12. Zhuang HM, Cortés-Blanco A, Pourdehnad M, et al. Do high glucose levels have differential effect on FDG uptake in inflammatory and malignant disorders? *Nucl Med Commun.* 2001;22:1123–1128.
13. De Winter F, Van De Wiele C, Vogelaers D, De Smet K, Verdonk B, Dierckx RA. Fluorine-18 fluorodeoxyglucose positron emission tomography: a highly accurate imaging modality for the diagnosis of chronic musculoskeletal infections. *J Bone Joint Surg Am.* 2001;83:651–660.
14. Mader JT, Wilson KJ. Comparative evaluation of cefamandole and cephalothin in the treatment of experimental *Staphylococcus aureus* osteomyelitis in rabbits. *J Bone Joint Surg Am.* 1983;65:507–513.
15. Kubota R, Yamada S, Kubota K, Ishiwata K, Tamahashi N, Ido T. Intratumoral distribution of fluorine-18-fluorodeoxyglucose in vivo: high accumulation in macrophages and granulation tissue studied by microautoradiography. *J Nucl Med.* 1992;33:1972–1980.
16. Meyer M, Gast T, Raja S, Hubner K. Increased F-18 FDG accumulation in an acute fracture. *Clin Nucl Med.* 1994;19:13–14.
17. Zhuang H, Duarte PS, Pourdehand M, Shnier D, Alavi A. Exclusion of chronic osteomyelitis with F-18 fluorodeoxyglucose positron emission tomography imaging. *Clin Nucl Med.* 2000;25:281–284.
18. Zhuang H, Sam JS, Chacko TK, et al. Rapid normalization of osseous FDG uptake following traumatic or surgical fractures. *Eur J Nucl Med Mol Imaging.* 2003;30:1096–1103.
19. Calhoun JH, Mader JT. Treatment of osteomyelitis with a biodegradable antibiotic implant. *Clin Orthop.* 1997;341:206–214.
20. Mader JT. Animal models of osteomyelitis. *Am J Med.* 1985;78:213–217.
21. Lew DP, Waldvogel FA. Osteomyelitis. *N Engl J Med.* 1997;336:999–1007.
22. Norden CW, Keleti E. Experimental osteomyelitis caused by *Pseudomonas aeruginosa. J Infect Dis.* 1980;141:71–75.
23. Schmitz A, Risse JH, Textor J, et al. FDG-PET findings of vertebral compression fractures in osteoporosis: preliminary results. *Osteoporos Int.* 2002;12:755–761.